

Journal of Materials Chemistry A

Accepted Manuscript



This is an *Accepted Manuscript*, which has been through the Royal Society of Chemistry peer review process and has been accepted for publication.

Accepted Manuscripts are published online shortly after acceptance, before technical editing, formatting and proof reading. Using this free service, authors can make their results available to the community, in citable form, before we publish the edited article. We will replace this *Accepted Manuscript* with the edited and formatted *Advance Article* as soon as it is available.

You can find more information about *Accepted Manuscripts* in the [Information for Authors](#).

Please note that technical editing may introduce minor changes to the text and/or graphics, which may alter content. The journal's standard [Terms & Conditions](#) and the [Ethical guidelines](#) still apply. In no event shall the Royal Society of Chemistry be held responsible for any errors or omissions in this *Accepted Manuscript* or any consequences arising from the use of any information it contains.

Cite this: DOI: 10.1039/c0xx00000x

www.rsc.org/xxxxxx

ARTICLE TYPE

Investigation of the effect of large aromatic fusion in the small molecule backbone on the solar cell device fill factor

Huanran Feng,^{‡,a} Miaomiao Li,^{‡,a} Wang Ni,^a Feng Liu,^b Xiangjian Wan,^{*a} Bin Kan,^a Yunchuang Wang,^a Yamin Zhang,^a Qian Zhang,^a Yi Zuo,^a Xuan Yang,^a Yongsheng Chen^{*,a}

Received (in XXX, XXX) XthXXXXXXXXXX 20XX, Accepted Xth XXXXXXXXXXXX 20XX

DOI: 10.1039/b000000x

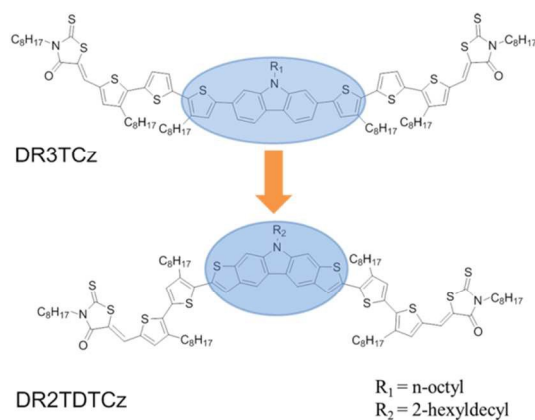
The structure and performance relationship in photovoltaic cells is still not fully understood, particularly in the case of controlling/optimizing the fill factor (FF). Here a pair of molecules DR2TDCz and DR3TCz with similar backbone structures varying conjugated central units were designed and synthesized, and their photovoltaic performance was studied and compared. The molecule DR2TDCz, containing dithieno[3,2-b;6,7-b]carbazole (DTCz) as the central unit, with a carbazole ring in the center and two fused thiophene rings at the two sides of carbazole, exhibits improved solar light absorption and slightly narrow band gap, compared with the analogue system DR3TCz which has carbazole and two unfused thiophene rings in the center. More importantly, it is found that introducing DTCz with thiophene fused 2,7-carbazole to replace 2,7-carbazole achieves a better molecular packing and favorable orientation, and thus benefiting charge transport. As a result, the DR2TDCz based device exhibits a power conversion efficiency (PCE) up to 7.03% with an impressively high FF of 75%, while the DR3TCz based device shows a PCE of 4.08% with a much lower FF of 54%. The results indicate that the FF can be tuned directly by the molecular structures and enlarged conjugation central core units could be beneficial to achieve high FF for the devices based on the acceptor-donor-acceptor (A-D-A) type small molecules.

1 Introduction

Organic photovoltaic cells (OPVs) are considered to be one of the most promising candidates for the next generation energy sources, having the advantages of being solution processable, light weight, low cost and flexible.¹⁻³ Over the past few years, extensive research efforts have been made on bulk heterojunction (BHJ) OPVs to improve their performance.⁴⁻¹¹ Currently, power conversion efficiencies (PCEs) around 10% have been reported for solar cells based on polymer based OPVs (P-OPVs) donors.¹²⁻¹⁷ Meanwhile, solution processed small molecule based OPVs (SM-OPVs) have demonstrated attractive advantages of small molecules, including well defined structure and no batch-to-batch variation and drawn more and more great attention.¹⁸⁻²³ So far significant progress has been made for SM-OPVs and PCEs of ~9% and ~10% have been achieved for single and tandem devices, respectively,²⁴⁻²⁶ indicating that the performance of SM-OPVs is indeed comparable with that of P-OPVs.

Considering the versatility of small molecules and relative short history of solution processed SM-OPVs, it is believed that higher performance can be obtained through molecule design and device optimization. From the equation of $PCE = V_{oc} \times J_{sc} \times FF / P_{in}$, to obtain an outstanding PCE, the three parameters

including open circuit voltage (V_{oc}), short circuit current (J_{sc}) and fill factor (FF) should be optimized simultaneously. Generally, SM-OPVs exhibit higher V_{oc} than that of P-OPVs. However, J_{sc} and FF, especially the latter, are the parameters that are difficult to control and improve. Low FF has been regarded as one of the bottlenecks for solution processed SM-OPVs. The value of FF with 60% has not realized until 2012.²⁷ Currently, only a few examples with the FF value over 70% have been reported.^{24-26, 28-32} As a parameter describing the quality of the solar cells, FF is determined by many factors, such as charge mobility, the balance of electron and hole mobilities, charge recombination, series and shunt resistances, etc.^{33, 34} To realize high FF, the donor material design,³⁵⁻³⁷ is the first step since the initial morphology formation with the acceptors in the active layers is determined by the donor intrinsic packing modes, miscibility and phase separation with acceptors.¹⁶ Together with the next step, device optimization process such as incorporation of additives, thermal annealing, and interface layer engineering, high FF is expected to achieve. However, tuning or controlling FF seems quite challenging and sometimes quite unexpected results could be obtained.³⁸⁻⁴² Previous studies have indicated that large fusion systems with fused polycyclic aromatic units, can largely suppress inter annular rotation, and thus enhance the π -electron delocalization and promote cofacial



Scheme 1 Chemical structures of DR3TCz and DR2TDTcZ.

π - π stacking. This may improve the properties of light absorption and charge transport, and these are expected to improve the FF in most cases.⁴³⁻⁴⁸ In addition, carbazole is one of the most important aromatic units for designing high performance polymers for light emitting diodes, organic field effect transistors and photovoltaic cells.^{49, 50} Generally, due to the weak electron-donating ability of carbazole unit, carbazole based polymers possess deep highest occupied molecular orbital (HOMO) energy levels, which are important for realizing high V_{oc} . Recently, small molecules with carbazole units were applied to OPVs and showed high V_{oc} , but relatively low FF.^{51, 52}

Considering the above mentioned factors and our previous work^{32, 53-56}, we designed and synthesized a new A-D-A small molecule DR2TDTcZ with a larger fusion central unit, where a dithieno[3,2-b;6,7-b]carbazole(DTCz) unit is used as the donor core unit, consisting of carbazole in the center and two thiophene rings fused at the ends of carbazole to enlarge the planar conjugation (Scheme 1). Also, DTCz based polymers with high mobility have been used for organic optoelectronic studies with outstanding performance.^{57, 58} As a comparison, a small molecule DR3TCz with carbazole as the central core without such large fusion but similar backbone structure was synthesized to investigate the effect of larger fused aromatic system. The solar cells fabricated with DR3TCz:PC₇₁BM and DR2TDTcZ:PC₇₁BM blends both exhibit similar high V_{oc} over 0.9 V. However, their PCEs, especially the FFs of the two molecules based devices are markedly different. The device based on DR3TCz exhibits a PCE of 4.08% with a low FF of 54%, while the device with DR2TDTcZ shows a high PCE of 7.03%, with an impressively high FF of 75%, which is one of the highest values in OPVs.^{25, 28, 31, 59, 60} The results indicate that the FF could be tuned and enhanced with enlarged conjugation central core units.

2 Experimental

2.1 Synthesis of DR3TCz and DR2TDTcZ

Detailed synthetic schemes for the two materials can be found in the ESI[†]. All reactions and manipulations were carried out under argon atmosphere with the use of standard Schlenk techniques. All starting materials, unless otherwise specified, were purchased from commercial suppliers and used without further purification. N-(n-octyl)-2,7-dibromocarbazole and N-(2-hexyldecyl)-

dithieno[2,3-b;7,6-b]carbazole were prepared according to the reported methods.^{58, 63}

2.2 Measurements and instruments

The ¹H and ¹³C nuclear magnetic resonance (NMR) spectra were taken on a Bruker AV400 Spectrometer. Matrix assisted laser desorption/ionization time-of-flight mass spectrometry (MALDI-TOF MS) was performed on a Bruker Autoflex III instrument. Transmission electron microscopy (TEM) was performed on a Philips Technical G2 F20 at 200 kV. Thermo gravimetric analyses (TGA) were carried out on a NETZSCH STA 409PC instrument under a purified nitrogen gas flow with a 10 °C min⁻¹ heating rate. UV-vis spectra were obtained with a JASCO V-570 spectrophotometer. The GIWAXS (grazing incidence wide angle X-ray scattering) and Resonant soft X-ray scattering (RSoXS) were performed at beamline 7.3.3 and 11.0.1.2 at Lawrence Berkeley National Lab. Atomic force microscope (AFM) investigation was performed using a Bruker MultiMode 8 instrument in the "tapping" mode. Cyclic voltammetry (CV) experiments were performed with a LK98B II Microcomputer-based Electrochemical Analyzer in dichloromethane solutions. All measurements were carried out at room temperature with a conventional three-electrode configuration using a glassy carbon electrode as the working electrode, a saturated calomel electrode (SCE) as the reference electrode, and a Pt wire as the counter electrode. The dichloromethane was distilled from calcium hydride under dry argon immediately prior to use. Tetrabutylammonium phosphorus hexafluoride (Bu₄NPF₆, 0.1 M) in dichloromethane was used as the supporting electrolyte, the molecules were dissolved in the above dichloromethane solution before measurement, and the scan rate was 100 mV s⁻¹.

The current density-voltage (J - V) characteristics of photovoltaic devices were obtained by a Keithley 2400 source-measure unit. The photocurrent was measured under simulated illumination of 100 mW cm⁻² with AM1.5G irradiation using a xenon-lamp-based solar simulator [Oriel 96000 (AM1.5G)] in an argon-filled glove box. Simulator irradiance was characterized using a calibrated spectrometer, and illumination intensity was set using a certified silicon diode. External quantum efficiency values (EQEs) of the encapsulated devices were obtained with a halogen tungsten lamp, monochromator, optical chopper, and lock-in amplifier in air and the photon flux was determined by a calibrated silicon photodiode.

SCLC mobility was measured using a diode configuration of ITO/PEDOT:PSS/donor:PC₇₁BM/Au for hole mobility and ITO/Al/donor:PC₇₁BM/Al for electron mobility and fitting the results to a space charge limited form, where SCLC is described by:

$$J = \frac{9\epsilon_0\epsilon_r\mu_0V^2}{8L^3}$$

where J is the current density, L is the film thickness of the active layer, μ_0 is the mobility, ϵ_r is the relative dielectric constant of the transport medium, ϵ_0 is the permittivity of free space (8.85×10^{-12} F m⁻¹), V ($= V_{\text{appl}} - V_{\text{bi}}$) is the internal voltage in the device, where V_{appl} is the applied voltage to the device and V_{bi} is the built-in voltage due to the relative work function difference of the two electrodes.

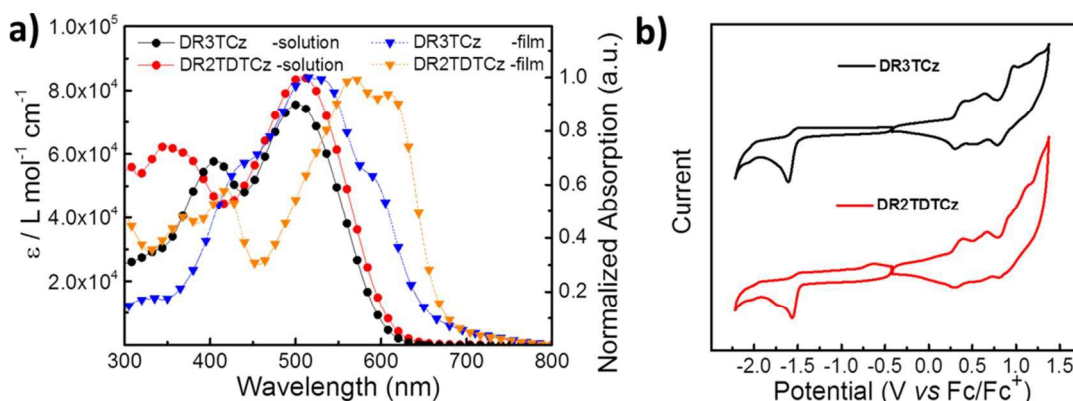


Fig. 1a) Absorption spectra of DR3TCz and DR2TDCz in chloroform solution and as-cast films. **b)** Cyclic voltammograms of DR3TCz and DR2TDCz in dichloromethane solution of 0.1 mol L⁻¹ Bu₄NPF₆ with a scan rate of 100 mV s⁻¹.

Table 1 Optical and electrochemical data of DR3TCz and DR2TDCz.

Compound	$\lambda_{\max, \text{sol}}$ (nm)	ϵ_{sol} (L mol ⁻¹ cm ⁻¹)	$\lambda_{\max, \text{film}}$ (nm)	$E_{\text{g}}^{\text{opt, film}}$ (eV)	E_{g}^{CV} (eV)	HOMO ^{CV} (eV)	LUMO ^{CV} (eV)
DR3TCz	502	7.6×10^4	516	1.88	1.80	-5.08	-3.28
DR2TDCz	507	8.1×10^4	567	1.82	1.74	-5.05	-3.31

2.3 Fabrication of photovoltaic cells

The photovoltaic devices were fabricated with a structure of glass/ITO/PEDOT:PSS/donor:acceptor/ETL-1/Al. The ITO-coated glass substrates were cleaned by ultrasonic treatment in detergent, deionized water, acetone, and isopropyl alcohol under ultrasonication for 15 minutes each time and subsequently dried by a nitrogen flow. A thin layer of PEDOT:PSS (Baytron P VP Al 4083, filtered at 0.45 μm) was spin-coated (3000 rpm, ca. 40 nm thick) onto the ITO surface. After baked at 150 °C for 20 min, the substrates were transferred into an argon filled glove box. Subsequently, the active layer was spin-coated from blend chloroform solutions with the weight ratio of DR3TCz or DR2TDCz and PC₇₁BM at 1:0.8 (or other ratios) and then annealed at 80 °C for 10 min. After cooling to the room temperature, the substrates were placed in a glass petri dish containing 150 μL chloroform for 60 s for solvent vapor annealing. Then the substrates were removed. And ETL-1 solution (0.5 mg/ml, dissolved in methanol) was spin-coated at 3000 rpm, a 50 nm Al layer was deposited on the ETL-1 film under high vacuum (1×10^{-4} Pa) with a deposition rate of 0.5 $\text{\AA}\text{s}^{-1}$. The effective area of each cell was 4 mm² as defined by masks for the solar cell devices discussed in this work.

3. Results and Discussion

3.1 Synthesis and Thermal Stability

The synthesis of DR3TCz and DR2TDCz is shown in Scheme S1 with details described in ESI[†]. Compound **5** was prepared following the literature method.⁵⁸ As shown in Scheme S1, the intermediate DCHO2TDCz was synthesized by a Stille coupling reaction between **6** and 5'-bromo-3,4'-dioctyl-2,2'-bithiophene-5-carbaldehyde under argon atmosphere in the presence of Pd(PPh₃)₄ as the catalyst for 24 h. DCHO3TCz was prepared

according to the reported method.⁵⁵ The target molecules were obtained by the Knoevenagel condensation of their corresponding donor unit precursors DCHO2TDCz and DCHO3TCz with 3-octylrhodanine in the presence of pyridine. The thermal stability of these compounds was investigated by thermal gravimetric analysis (TGA) (see Fig. S1). The results reveal that the onset decomposition temperatures of the compounds are all around 330 °C under N₂ atmosphere, indicating that they are quite thermally stable and can be used for device fabrication.

3.2 Optical Properties and Electrochemical Properties

The UV-vis absorption spectra of DR3TCz and DR2TDCz in chloroform solution and in the solid state are shown in Fig. 1a. The detailed absorption data, including the absorption maxima in solution and film as well as the optical band gap, are summarized in Table 1. DR3TCz in chloroform solution shows a maximum absorption peak at 502 nm with an absorption coefficient of 7.6×10^4 L mol⁻¹ cm⁻¹. After fusing the two thiophene rings with the carbazole unit, though with the same total conjugation length, DR2TDCz in chloroform solution shows a slightly bathochromic absorption peak at 507 nm, with a higher maximal coefficient of 8.1×10^4 L mol⁻¹ cm⁻¹ compared with that of DR3TCz. In the solid state, compared with the absorption peak (516 nm) of the DR3TCz film which is red-shifted by only 11 nm relative to the solution absorption, DR2TDCz (567 nm) shows much clearer bathochromic shift about 60 nm. And another sharp absorption peak at 610 nm is observed for the DR2TDCz film, suggesting vibronic progression due to a rigid coplanarization and more effective π - π mode stacking of the larger fused systems in DR2TDCz in the solid state.^{62, 63} By extrapolation of the absorption onsets in the film state, the optical band gap of DR2TDCz is estimated to be 1.82 eV, which is lower than that of DR3TCz (1.88 eV).

The electrochemical properties of DR3TCz and DR2TDCz were investigated by cyclic voltammetry (CV). Ferrocene/ferrocenium of the (Fc/Fc⁺) redox couple (4.8 eV

below the vacuum level) was used as the internal calibration. As shown in Fig.1b, the HOMO and LUMO energy levels, which are -5.08 and -3.28 eV for DR3TCz and -5.05 and -3.31 eV for DR2TDTcZ, respectively, were calculated from the onset oxidation and reduction potential. The electrochemical band gaps of DR3TCz and DR2TDTcZ are estimated to be 1.80 eV and 1.74 eV, respectively. Herein, the CV band gaps of the two molecules are lower than their corresponding optical band gaps, which might be caused by the measurement conditions. The CV measurement was conducted in the corresponding molecules dichloromethane solutions. While the optical band gaps were estimated from the sample solid film absorption.

3.3 Photovoltaic Properties

With the basic properties characterized for these two donor molecules, BHJ organic solar cells were fabricated using them as the electron donor and PC₇₁BM as the electron acceptor materials with a device structure of glass/ITO/PEDOT:PSS/donor:acceptor/ETL-1/Al, using the conventional solution spin-coating process. ETL-1, used as the interfacial layer for cathodes, is a methanol soluble fullerene surfactant developed by Alex K.-Y.,⁶⁴ and its structure is shown in Fig. S5. The corresponding optimized parameters with donor:acceptor ratio of 1:0.8 (w/w) are summarized in Table 2. The optimum current density vs voltage (J - V) curves measured under AM 1.5G irradiation at the intensity of 100 mWcm⁻² are shown in Fig.2a. The device based on DR3TCz without post treatment shows only a PCE of 1.48%, with a V_{oc} of 1.03 V, a J_{sc} of 4.78 mA cm⁻², and a FF of 30%. The device based on DR2TDTcZ:PC₇₁BM exhibits a V_{oc} of 0.93 V, a J_{sc} of 5.98 mA cm⁻², and a FF of 48%, also resulting in a low PCE of 2.70%. The low J_{sc} and FF of the devices are attributed to the un-optimized morphologies of the photovoltaic layers, which can be seen from the atomic force microscope (AFM) and transmission electron microscopy (TEM) images, as discussed below. After thermal and solvent annealing to optimize the active layer morphology, the device performances of DR3TCz and DR2TDTcZ were both improved significantly, attributed to the significant increase in J_{sc} and FF as shown in Table 2. Particularly, the OPV devices based on DR2TDTcZ:PC₇₁BM exhibits a PCE of 7.03% with a remarkable FF of 75%, one of the highest values of FF in OPVs so far, whereas the FF of the device with DR3TCz is only 54%, resulting in a relatively low PCE of 4.08%. Considering the same

device structure and processing treatment, the improved FF of DR2TDTcZ was more likely attributed to the molecular structures related to the film morphology and molecular packing, as discussed in detail below. Moreover, the solar cells fabricated with DR3TCz:PC₇₁BM and DR2TDTcZ:PC₇₁BM blends both achieve high V_{oc} over 0.9V. The higher V_{oc} of DR3TCz based device is consistent with its lower HOMO (-5.08 eV) level compared with that (-5.05 eV) of DR2TDTcZ. Compared with the DR3TCz based device, the device based on DR2TDTcZ exhibits a lower series resistance (5 vs 29 Ω cm²) and a higher shunt resistance (1075 vs 356 Ω cm²), which indicates better ohmic contact in the DR2TDTcZ based device. The external quantum efficiency (EQE) curves of the best devices based on DR3TCz and DR2TDTcZ are shown in Fig.2b, where the devices with DR3TCz and DR2TDTcZ exhibit photo-to-current responses from 300 to 710 nm with the maximum EQE value reaching 56% and 59%, respectively. In addition, the device based on DR2TDTcZ shows much higher EQE at the wavelength over 550 nm relative to that of DR3TCz based device, which is consistent with the absorption spectra of the blend films.

To further understand the high performance of DR2TDTcZ based device and the significant differences with DR3TCz based device, the relationship of the photocurrent (J_{ph}) and effective voltage (V_{eff}) or light intensity (P_{in}) is shown in Fig.3. Fig.3a displays the dependence of the photocurrent density J_{ph} ($J_{ph} = J_L - J_D$) on the effective voltage V_{eff} ($V_{eff} = V_0 - V_a$), in which J_L and J_D are the current density under illumination and in the dark, respectively, V_a is the applied voltage, and V_0 is the voltage at which $J_{ph} = 0$.^{65, 66} From Fig.3a, with increasing V_{eff} , the saturation photocurrent (J_{sat}) in the device with DR2TDTcZ was reached earlier than that in the device based on DR3TCz. This suggests that for DR2TDTcZ based devices, both the processes of photo generated exciton's dissociation into free charge and the charge collection at the electrodes are more efficient with little geminate and bimolecular recombination. In addition, J_{sat} is generally correlated to the maximum exciton generation rate (G_{max}), which is a measure of the maximum number of photons absorbed.¹⁴ A higher J_{sat} was observed in the DR2TDTcZ based device, which is in agreement with the UV-vis absorption results discussed above. The ratio of J_{ph}/J_{sat} can be used to judge the overall exciton dissociation efficiency and charge collection efficiency.⁶⁷ Fig.3b shows the plot of the normalized photocurrent (J_{ph}/J_{sat}) in the devices fabricated with the two donor molecules.

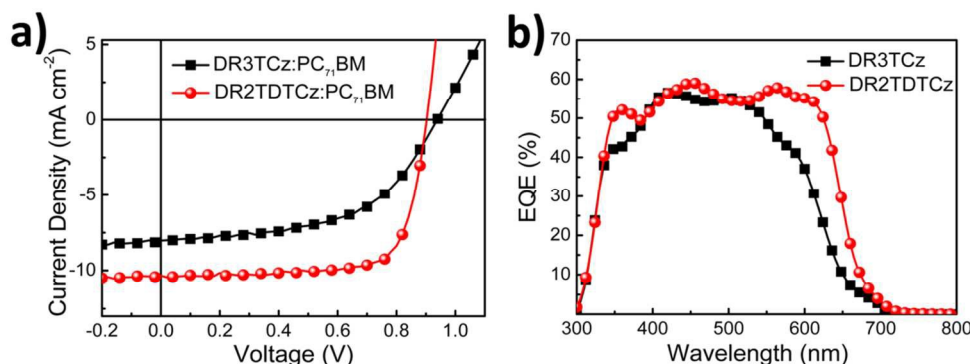


Fig.2 Device performance with the structure of ITO/PEDOT:PSS/donor:PC₇₁BM/ETL-1/Al. a) Current density-voltage (J - V) characteristics of both devices under the optimized conditions and AM 1.5G irradiation (100 mW cm⁻²). b) The external quantum efficiency (EQE) curves for both devices.

Table 2 The photovoltaic performance of DR3TCz and DR2TDTCz based devices.

Donor:PC ₇₁ BM (w:w)	V_{oc} (V)	$J_{sc}(J_{sc}^c)$ (mA cm ⁻²)	FF(FF ^c) (%)	PCE _{best} (PCE _{ave} ^c) (%)	R _s (Ω)	R _{sh} (Ω)
DR3TCz:PC ₇₁ BM (1:0.8) ^a	1.03	4.32(4.17)	29(28)	1.29(1.20)	162	287
DR3TCz:PC ₇₁ BM (1:0.8) ^b	0.94	8.02(7.91)	54(53)	4.08(3.94)	29	356
DR2TDTCz:PC ₇₁ BM (1:0.8) ^a	0.93	5.98(5.91)	48(47)	2.70(2.58)	14	274
DR2TDTCz:PC ₇₁ BM (1:0.8) ^b	0.90	10.34(10.13)	75(74)	7.03(6.75)	5	1075

^awithout post treatment; ^b with two step annealing treatment; ^c the average performance parameter is obtained from 40 devices.

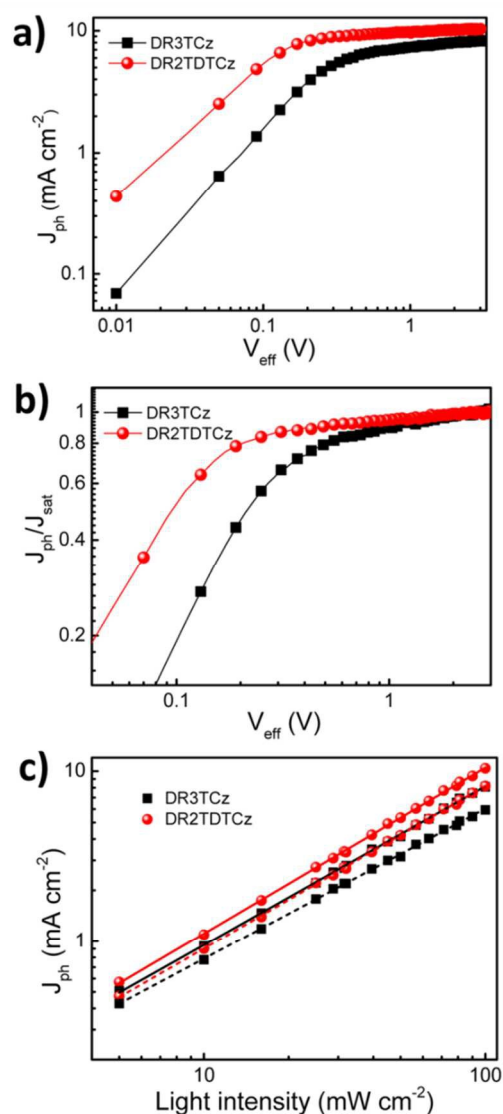


Fig.3a) and b) Photocurrent density and charge collection efficiency versus effective voltage (J_{ph} - V_{eff}) characteristics for both devices under AM 1.5G irradiation (100 mW cm⁻²). c) Double logarithmic plots of photocurrent density as a function of the incident light intensity for DR2TDTCz based (square) and DR3TCz based (circle) devices under the saturation photocurrent conditions (solid line) and the maximal power output conditions (dashed line). The lines represent the fitting curves.

The values of J_{ph}/J_{sat} are 89% and 93% for DR3TCz and DR2TDTCz based devices, respectively, under the short circuit conditions. At the maximal power output conditions, the ratios of DR3TCz and DR2TDTCz based devices are 66% and 81%, respectively. The results indicate that the device with DR2TDTCz possesses higher exciton dissociation efficiency and charge collection efficiency.⁶⁷

The values of J_{ph} of the OPV devices at various illumination intensities were measured to examine charge transport and bimolecular recombination. In general, the value of J_{sc} of an OPV device follows a power law dependence with respect to P_{in} (i.e., $J_{ph} \propto P_{in}^\alpha$). When the build-up of space charges reaches a fundamental limit, the exponential factor (α) is 3/4, and if there is no space charge build-up, $\alpha=1$.⁶⁸ As shown in Fig.3c, under saturation photocurrent conditions, α are ~1 (0.93 for the DR3TCz based devices and 0.97 for DR2TDTCz based device). Under the maximal power output conditions, α is 0.95 for the DR2TDTCz based device, but it decreases to 0.88 for the DR3TCz based device. These results suggest little bimolecular recombination and build-up of space charge for the DR2TDTCz based device, but not for the DR3TCz case, due to higher and more balanced charge mobility (electron and hole) for the DR2TDTCz case discussed below.

3.4 Morphology, Molecular Ordering and Mobility

The active layer morphology was examined by atomic force microscope (AFM) and transmission electron microscopy (TEM). As shown in Fig.4, it is found that without post treatment, the films of DR3TCz and DR2TDTCz blended with PC₇₁BM show root-mean-square (*rms*) surface roughness of 0.72 and 2.56 nm, respectively, and after thermal and solvent vapor annealing, the *rms* roughness of the blend films increases to 2.94 nm for DR3TCz but decreases to 1.75 nm for DR2TDTCz, which reveals that the films are smooth with high quality. In addition, from TEM images (Fig.4), without post treatment, the DR3TCz based film appears homogeneous with a little phase separation, whereas some defined phase separation of the donor and acceptor was observed in DR2TDTCz blend. After annealing, better interpenetrating networks of donor and acceptor phases are observed for both DR3TCz- and DR2TDTCz based blend films, which are beneficial for charge transport. Overall, under the optimized conditions, the blend films for both two compounds demonstrate rather fine and evenly distributed domains with sizes

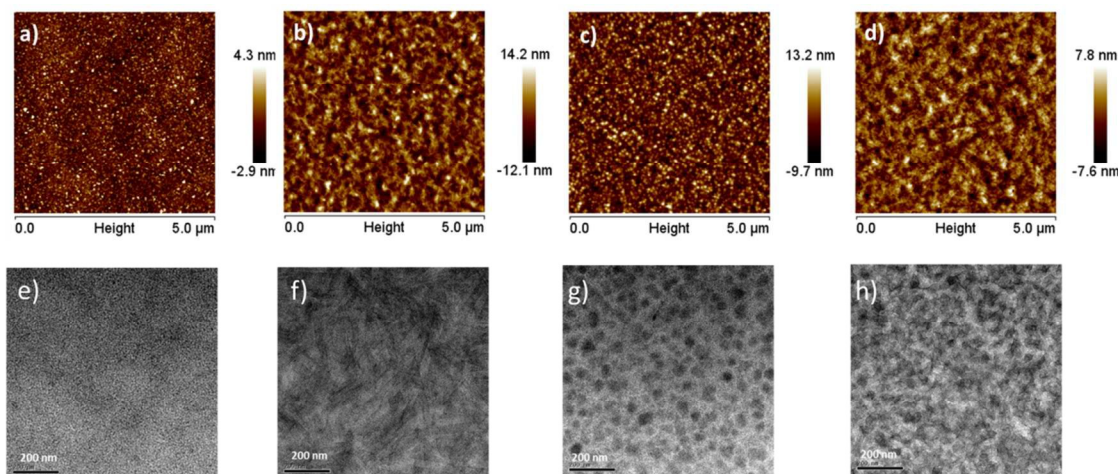


Fig.4 Tapping-mode AFM height images of (a, b) DR3TCz:PC₇₁BM blend films and (c, d) DR2TDTcZ:PC₇₁BM blend films and TEM images of (e, f) DR3TCz:PC₇₁BM blend films and (c, d) DR2TDTcZ:PC₇₁BM blend films. (a, c, e, g) without post treatment and (b, d, f, h) with thermal and solvent annealing.

of tens of nanometers and continuous interpenetrating networks without any observed large aggregates of either the donor or the acceptor.

In order to investigate the effect of large fused aromatic system on the molecular ordering at solid state, the nanoscale morphology of the blend films were characterized by grazing incidence wide angle X-ray scattering (GIWAXS) and Resonant soft X-ray scattering (RSoXS) (Fig.5, Fig.S3 and Table S1). As shown in the Fig. 5a, DR2TDTcZ:PC₇₁BM blend film, especially after annealing treatment, showed sharp (h00) reflections peaks corresponding to the distance between neighbouring backbones determined by side chain intercalation. For DR2TDTcZ:PC₇₁BM blend film, the lamellar spacing decreased for 18.7 Å ($q = 0.336 \text{ \AA}^{-1}$) to 15.4 Å ($q = 0.360 \text{ \AA}^{-1}$) after annealing. In addition, there existed (010) peak corresponding to π -stacking of the molecule backbone with distance around 3.7 Å ($q = 1.68 \text{ \AA}^{-1}$) only in the out of plane profile for DR2TDTcZ:PC₇₁BM film with annealing, indicating a great preference for face-on molecular orientation which is favorable for effective charge transport in photovoltaic devices. In contrast, DR3TCz:PC₇₁BM blend film showed broad (100) peaks with lamellar spacing 24.3 Å ($q = 0.251 \text{ \AA}^{-1}$) and 21.8 Å ($q = 0.288 \text{ \AA}^{-1}$) before and after annealing in the out of plane profile. There was a (010) peak with distance around 3.9 Å ($q = 1.60 \text{ \AA}^{-1}$) only in the in plane profile, indicating a preferred edge-on orientation. These results demonstrated that DR2TDTcZ with the larger aromatic fusion exhibited tendency to form more ordered molecule packing and higher crystallinity and favorable orientation, which could be benefit for increasing the charge transport, thus higher FF. On the other hand, RSoXS for the DR3TCz:PC₇₁BM blend film showed an interference ($q = 0.017 \text{ \AA}^{-1}$) corresponding to a domain center-to-center distance of 37 nm, which increased to 130 nm after the two steps annealing. For DR2TDTcZ:PC₇₁BM, the domain center-to-center distance only increased a little from 73 nm to 83 nm after the post treatment.

The mobilities of the blend films were measured by the space

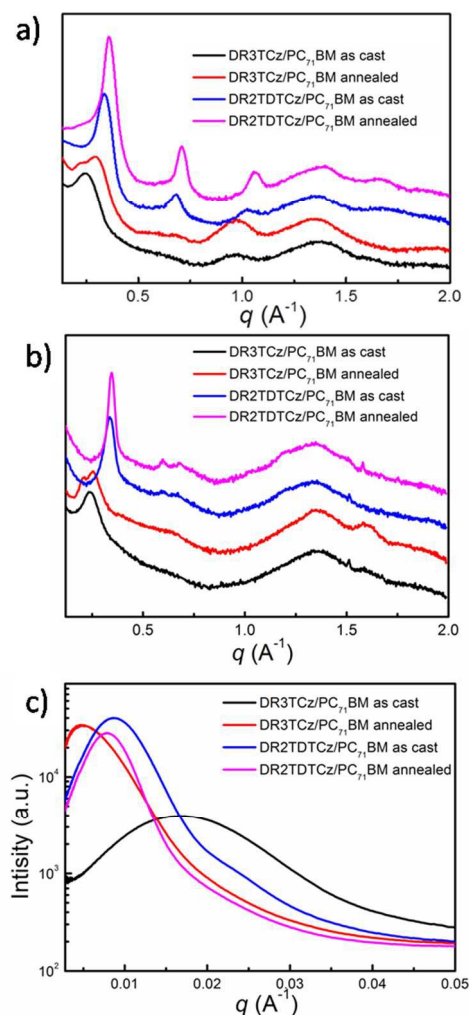


Fig.5a) Out-of-plane and b) in-plane line cut profiles of DR3TCz and DR2TDTcZ films as cast and treatment by thermal and solvent annealing in GIWAXS, c) RSoXS profiles of DR3TCz and DR2TDTcZ films as cast and treatment by thermal and solvent annealing.

Table 3 The hole and electron mobilities of DR3TCz:PC₇₁BM and DR2TDTcZ:PC₇₁BM based devices.

Donor	Without post treatment			With two step annealing treatment		
	μ_h (cm ² V ⁻¹ s ⁻¹)	μ_e (cm ² V ⁻¹ s ⁻¹)	μ_e/μ_h	μ_h (cm ² V ⁻¹ s ⁻¹)	μ_e (cm ² V ⁻¹ s ⁻¹)	μ_e/μ_h
DR3TCz	3.78×10 ⁻⁵	7.37×10 ⁻⁵	1.95	8.44×10 ⁻⁵	1.44×10 ⁻⁴	1.71
DR2TDTcZ	9.10×10 ⁻⁵	1.17×10 ⁻⁴	1.28	3.22×10 ⁻⁴	3.75×10 ⁻⁴	1.16

charge limited current (SCLC) method, and the results are shown in Table 3 (curves are given as Fig. S4). The hole and electron mobilities of the devices based on DR3TCz:PC₇₁BM are 3.75×10⁻⁵ cm² V⁻¹ s⁻¹ and 7.37×10⁻⁵ cm² V⁻¹ s⁻¹ without post treatment, and improved to 8.44×10⁻⁵ cm² V⁻¹ s⁻¹ and 1.44×10⁻⁴ cm² V⁻¹ s⁻¹ with thermal and solvent vapor annealing, respectively. Similar to DR3TCz, after thermal and solvent treatment, DR2TDTcZ:PC₇₁BM based devices also present increased hole and electron mobilities from 9.01×10⁻⁵ cm² V⁻¹ s⁻¹ and 1.17×10⁻⁴ cm² V⁻¹ s⁻¹ without annealing to 3.22×10⁻⁴ cm² V⁻¹ s⁻¹ and 3.75×10⁻⁴ cm² V⁻¹ s⁻¹, respectively. As can be seen, the devices based on DR2TDTcZ:PC₇₁BM show not only higher hole and electron mobilities without/with post treatment, but also more balanced hole and electron mobilities than the devices of DR3TCz:PC₇₁BM. All these should result in less bimolecular recombination and build-up of space charge, and thus higher J_{sc} and FF in DR2TDTcZ based device. The significantly higher hole mobility of DR2TDTcZ is expected due to the more ordered packing mode, higher crystallinity and favorable face on orientation of DR2TDTcZ in the films as observed from the above TEM and GIWAXS analysis.

4. Conclusion

In conclusion, we have designed and synthesized two structurally comparable small-molecule donors, DR3TCz and DR2TDTcZ, as donors for solution processed SM-OPV. With an enlarged fused π central unit, DR2TDTcZ shows significantly better FF and overall OPV performance than DR3TCz, which could be attributed to the better packing and favorable orientation caused by the large fused central core unit, thus benefit charge transport in DR2TDTcZ based devices. It is believed that the impressively high FF of 75% for DR2TDTcZ based devices is associated directly with the increased large π - π fusion system, indicating using larger fusion to enlarge central building blocks could be an effective strategy to obtain high FF for A-D-A structure SM-OPV.

Acknowledgments

The authors gratefully acknowledge the financial support from MoST (2014CB643502), NSFC (51373078, 51422304, 91433101), PCSIRT (IRT1257) and Tianjin city (13RCGFGX01121). Portions of morphological characterization of the active layers were carried out at the Advanced Light Source, Berkeley National Laboratory, which was supported by the DOE-funded Energy Frontier Research Center on Polymer Based Materials for Harvesting Solar Energy (DE-SC0001087). The authors also thank beam line BL14B1 (Shanghai Synchrotron Radiation Facility) for providing the beam time.

Notes and references

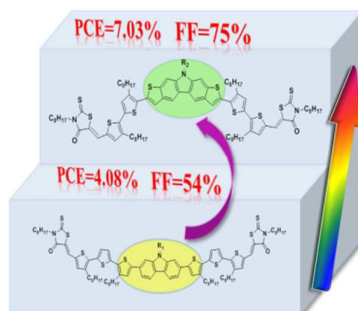
- ⁵⁰ ^aState Key Laboratory and Institute of Elemento-Organic Chemistry and Centre for Nanoscale Science and Technology, Institute of Polymer Chemistry, College of Chemistry, Collaborative Innovation Center of Chemical Science and Engineering (Tianjin), College of Chemistry, Nankai University, Tianjin, 300071, China. Fax: 86(22) 2349 9992
- ⁵⁵ Email dress: xjwan@nankai.edu.cn, yschen99@nankai.edu.cn.
- ^bMaterials Sciences Division, Lawrence Berkeley National Laboratory, Berkeley, CA 94720, USA
- † Electronic Supplementary Information (ESI) available: Synthesis and characterization, 2D GI-WAXS data, SCLC figures, UV-vis absorption spectra of the blended films. See DOI:10.1039/b000000x/
- ‡ These authors contribute equally to this work.
- G. Yu, J. Gao, J. C. Hummelen, F. Wudl and A. J. Heeger, *Science*, 1995, **270**, 1789.
 - L.-M. Chen, Z. Hong, G. Li and Y. Yang, *Adv. Mater.*, 2009, **21**, 1434.
 - B. C. Thompson and J. M. J. Frechet, *Angew. Chem. Int. Ed.*, 2008, **47**, 58.
 - J. E. Coughlin, Z. B. Henson, G. C. Welch and G. C. Bazan, *Acc. Chem. Res.*, 2013, **47**, 257.
 - Y.-J. Cheng, S.-H. Yang and C.-S. Hsu, *Chem. Rev.*, 2009, **109**, 5868.
 - L. Ye, S. Zhang, L. Huo, M. Zhang and J. Hou, *Acc. Chem. Res.*, 2014, **47**, 1595.
 - J. Mei and Z. Bao, *Chem. Mater.*, 2013, **26**, 604.
 - D. Demeter, T. Rousseau, P. Leriche, T. Cauchy, R. Po and J. Roncali, *Adv. Funct. Mater.*, 2011, **21**, 4379.
 - N. D. Eisenmenger, G. M. Su, G. C. Welch, C. J. Takacs, G. C. Bazan, E. J. Kramer and M. L. Chabynyc, *Chem. Mater.*, 2013, **25**, 1688.
 - X. Zhang, H. Bronstein, A. J. Kronemeijer, J. Smith, Y. Kim, R. J. Kline, L. J. Richter, T. D. Anthopoulos, H. Sirringhaus, K. Song, M. Heaney, W. Zhang, I. McCulloch and D. M. DeLongchamp, *Nat Commun*, 2013, **4**.
 - Z. B. Henson, K. Mullen and G. C. Bazan, *Nat Chem*, 2012, **4**, 699.
 - S.-H. Liao, H.-J. Jhuo, Y.-S. Cheng and S.-A. Chen, *Adv. Mater.*, 2013, **25**, 4766.
 - L. Ye, S. Zhang, W. Zhao, H. Yao and J. Hou, *Chem. Mater.*, 2014, **26**, 3603.
 - Z. He, C. Zhong, S. Su, M. Xu, H. Wu and Y. Cao, *Nat. Photonics*, 2012, **6**, 591.
 - J. You, L. Dou, K. Yoshimura, T. Kato, K. Ohya, T. Moriarty, K. Emery, C.-C. Chen, J. Gao, G. Li and Y. Yang, *Nat. Commun.*, 2013, **4**, 1446
 - Y. Liu, J. Zhao, Z. Li, C. Mu, W. Ma, H. Hu, K. Jiang, H. Lin, H. Ade and H. Yan, *Nat Commun*, 2014, **5**, 5293
 - J.-D. Chen, C. Cui, Y.-Q. Li, L. Zhou, Q.-D. Ou, C. Li, Y. Li and J.-X. Tang, *Adv. Mater.*, 2014, **27**, 1035.

18. J. Roncali, *Acc. Chem. Res.*, 2009, **42**, 1719.
19. S. Shen, P. Jiang, C. He, J. Zhang, P. Shen, Y. Zhang, Y. Yi, Z. Zhang, Z. Li and Y. Li, *Chem. Mater.*, 2013, **25**, 2274.
20. H. Zhou, L. Yang, A. C. Stuart, S. C. Price, S. Liu and W. You, *Angew. Chem. Int. Ed.*, 2011, **50**, 2995.
21. A. K. K. Kyaw, D. H. Wang, D. Wynands, J. Zhang, N. Thuc-Quyen, G. C. Bazan and A. J. Heeger, *Nano Lett.*, 2013, **13**, 3796.
22. H.-W. Lin, J.-H. Chang, W.-C. Huang, Y.-T. Lin, L.-Y. Lin, F. Lin, K.-T. Wong, H.-F. Wang, R.-M. Ho and H.-F. Meng, *J. Mater. Chem. A*, 2014, **2**, 3709.
23. A. Mishra and P. Bäuerle, *Angew. Chem. Int. Ed.*, 2012, **51**, 2020.
24. B. Kan, Q. Zhang, M. Li, X. Wan, W. Ni, G. Long, Y. Wang, X. Yang, H. Feng and Y. Chen, *J. Am. Chem. Soc.*, 2014, **136**, 15529.
25. V. Gupta, A. K. K. Kyaw, D. H. Wang, S. Chand, G. C. Bazan and A. J. Heeger, *Sci. Rep.*, 2013, **3**.
26. Y. Liu, C.-C. Chen, Z. Hong, J. Gao, Y. Yang, H. Zhou, L. Dou, G. Li and Y. Yang, *Sci. Rep.*, 2013, **3**, 3356.
27. T. S. van der Poll, J. A. Love, T.-Q. Nguyen and G. C. Bazan, *Adv. Mater.*, 2012, **24**, 3646.
28. Y. Chen, Z. Du, W. Chen, Q. Liu, L. Sun, M. Sun and R. Yang, *Org. Electron.*, 2014, **15**, 405.
29. Y. Lin, L. Ma, Y. Li, Y. Liu, D. Zhu and X. Zhan, *Adv. Energy Mater.*, 2014, **4**, 13000626.
30. W. Ni, M. Li, X. Wan, H. Feng, B. Kan, Y. Zuo and Y. Chen, *RSC Adv.*, 2014, **4**, 31977.
31. K. Sun, Z. Xiao, S. Lu, W. Zajaczkowski, W. Pisula, E. Hanssen, J. M. White, R. M. Williamson, J. Subbiah, J. Ouyang, A. B. Holmes, W. W. H. Wong and D. J. Jones, *Nat. Commun.*, 2015, **6**, 6013.
32. Q. Zhang, B. Kan, F. Liu, G. Long, X. Wan, X. Chen, Y. Zuo, W. Ni, H. Zhang, M. Li, Z. Hu, F. Huang, Y. Cao, Z. Liang, M. Zhang, T. P. Russell and Y. Chen, *Nat Photon*, 2015, **9**, 35.
33. V. D. Mihailetschi, H. X. Xie, B. de Boer, L. J. A. Koster and P. W. M. Blom, *Adv. Funct. Mater.*, 2006, **16**, 699.
34. G. Li, R. Zhu and Y. Yang, *Nat. Photonics*, 2012, **6**, 153.
35. F. Baert, C. Cabanetos, A. Leliege, E. Kirchner, O. Segut, O. Aleveque, M. Allain, G. Seo, S. Jung, D. Tondelier, B. Geffroy, J. Roncali, P. Leriche and P. Blanchard, *J. Mater. Chem. C*, 2015, **3**, 390.
36. D. Demeter, V. Jeux, P. Leriche, P. Blanchard, Y. Olivier, J. Cornil, R. Po and J. Roncali, *Adv. Funct. Mater.*, 2013, **23**, 4854.
37. A. Leliege, C.-H. L. Regent, M. Allain, P. Blanchard and J. Roncali, *Chem. Commun.*, 2012, **48**, 8907.
38. C. M. Proctor, J. A. Love and T. Q. Nguyen, *Adv Mater*, 2014, **26**, 5957.
39. C. M. Proctor, S. Albrecht, M. Kuik, D. Neher and T.-Q. Nguyen, *Adv. Energy Mater.*, 2014, **4**, 1400230.
40. C. M. Proctor, C. Kim, D. Neher and T.-Q. Nguyen, *Adv. Funct. Mater.*, 2013, **23**, 3584.
41. D. Credgington, F. C. Jamieson, B. Walker, T.-Q. Nguyen and J. R. Durrant, *Adv. Mater.*, 2012, **24**, 2135.
42. A. Guerrero, S. Loser, G. Garcia-Belmonte, C. J. Bruns, J. Smith, H. Miyauchi, S. I. Stupp, J. Bisquert and T. J. Marks, *Phys. Chem. Chem. Phys.*, 2013, **15**, 16456.
43. J.-S. Wu, S.-W. Cheng, Y.-J. Cheng and C.-S. Hsu, *Chem. Soc. Rev.*, 2015, **44**, 1113.
44. H. J. Son, L. Lu, W. Chen, T. Xu, T. Zheng, B. Carsten, J. Strzalka, S. B. Darling, L. X. Chen and L. Yu, *Adv. Mater.*, 2013, **25**, 838.
45. J. E. Anthony, *Angew. Chem. Int. Ed.*, 2008, **47**, 452.
46. J. E. Anthony, *Chem. Rev.*, 2006, **106**, 5028.
47. Y. Ruiz-Morales, *The Journal of Physical Chemistry A*, 2002, **106**, 11283.
48. H. Zhong, Z. Li, F. Deledalle, E. C. Fregoso, M. Shahid, Z. Fei, C. B. Nielsen, N. Yaacobi-Gross, S. Rossbauer, T. D. Anthopoulos, J. R. Durrant and M. Heeney, *J. Am. Chem. Soc.*, 2013, **135**, 2040.
49. J. F. Morin, M. Leclerc, D. Ades and A. Siove, *Macromol. Rapid Commun.*, 2005, **26**, 761.
50. N. Blouin and M. Leclerc, *Acc. Chem. Res.*, 2008, **41**, 1110.
51. M. Singh, R. Kurchania, J. A. Mikroyannidis, S. S. Sharma and G. D. Sharma, *J. Mater. Chem. A*, 2013, **1**, 2297.
52. P. Li, H. Tong, J. Ding, Z. Xie and L. Wang, *J. Mater. Chem. A*, 2013, **1**, 8805.
53. J. Zhou, X. Wan, Y. Liu, Y. Zuo, Z. Li, G. He, G. Long, W. Ni, C. Li, X. Su and Y. Chen, *J. Am. Chem. Soc.*, 2012, **134**, 16345.
54. Z. Li, G. He, X. Wan, Y. Liu, J. Zhou, G. Long, Y. Zuo, M. Zhang and Y. Chen, *Adv. Energy Mater.*, 2012, **2**, 74.
55. W. Ni, M. Li, B. Kan, Y. Zuo, Q. Zhang, G. Long, H. Feng, X. Wan and Y. Chen, *Org. Electron.*, 2014, **15**, 2285.
56. J. Zhou, Y. Zuo, X. Wan, G. Long, Q. Zhang, W. Ni, Y. Liu, Z. Li, G. He, C. Li, B. Kan, M. Li and Y. Chen, *J Am Chem Soc*, 2013, **135**, 8484.
57. Y. Chen, H. Tian, D. Yan, Y. Geng and F. Wang, *Macromolecules*, 2011, **44**, 5178.
58. Y. Deng, Y. Chen, J. Liu, L. Liu, H. Tian, Z. Xie, Y. Geng and F. Wang, *ACS App. Mater. Inter.*, 2013, **5**, 5741.
59. X. Guo, N. Zhou, S. J. Lou, J. Smith, D. B. Tice, J. W. Hennek, R. P. Ortiz, J. T. L. Navarrete, S. Li, J. Strzalka, L. X. Chen, R. P. H. Chang, A. Facchetti and T. J. Marks, *Nat Photon*, 2013, **7**, 825.
60. T. L. Nguyen, H. Choi, S. J. Ko, M. A. Uddin, B. Walker, S. Yum, J. E. Jeong, M. H. Yun, T. J. Shin, S. Hwang, J. Y. Kim and H. Y. Woo, *Energy Environ. Sci.*, 2014, **7**, 3040.
61. J.-F. Morin and M. Leclerc, *Macromolecules*, 2001, **34**, 4680.
62. M. Turbiez, P. Frere, M. Allain, C. Videlot, J. Ackermann and J. Roncali, *Chem. Eur. J.*, 2005, **11**, 3742.
63. C. Uhrich, R. Schueppel, A. Petrich, M. Pfeiffer, K. Leo, E. Brier, P. Kilickiran and P. Baeuerle, *Adv. Funct. Mater.*, 2007, **17**, 2991.
64. C.-Z. Li, C.-C. Chueh, H.-L. Yip, K. M. O'Malley, W.-C. Chen and A. K. Y. Jen, *J. Mater. Chem.*, 2012, **22**, 8574.
65. L. Lu, Z. Luo, T. Xu and L. Yu, *Nano Lett.*, 2012, **13**, 59.
66. P. W. M. Blom, V. D. Mihailetschi, L. J. A. Koster and D. E. Markov, *Adv. Mater.*, 2007, **19**, 1551.
67. Z. He, C. Zhong, X. Huang, W.-Y. Wong, H. Wu, L. Chen, S. Su and Y. Cao, *Adv. Mater.*, 2011, **23**, 4636.
68. M. Lenes, M. Morana, C. J. Brabec and P. W. M. Blom, *Adv. Funct. Mater.*, 2009, **19**, 1106.
69. P. Muller-Buschbaum, *Adv Mater*, 2014, **26**, 7692.

-
70. H. Sirringhaus, P. J. Brown, R. H. Friend, M. M. Nielsen, K. Bechgaard, B. M. W. Langeveld-Voss, A. J. H. Spiering, R. A. J. Janssen, E. W. Meijer, P. Herwig and D. M. de Leeuw, *Nature*, 1999, **401**, 685.

5

Graphical abstract



Molecules DR3TCz and DR2TDCz were synthesized and R2TDCz exhibits a PCE up to 7.03% with FF of 75%